Improving Drop Size and Velocity Estimates of an Optical Disdrometer: Implications for Sprinkler Irrigation Simulation

J. Burguete[1], E. Playán[1], J. Montero[2] and N. Zapata[1]

[1]: *Suelo y Agua. EEAD. CSIC. Zaragoza. Spain*

[2]: *Ingeniería Agroforestal. ETSIA. University of Castilla-La Mancha. Albacete. Spain*

Abstract

Optical disdrometers measure the attenuation of an infrared beam when water drops pass between the emitter and the receptor. The duration and intensity of the attenuation are used to estimate drop size and time of passage. These variables are used to calibrate and validate ballistic sprinkler simulation models. Two experimental problems affect the quality of the measurements: first, drops can pass through a side of the detector, so that only part of the drop attenuates the luminous flow; and second, several drops can overlap as they pass through the beam. This work presents a statistical treatment of the observed time of passage that can be used to eliminate a large part of the erroneous measurements, significantly improving the accuracy of disdrometer data. Furthermore, drop velocities can be estimated from the corrected times of passage. Simulation with the ballistic model shows that the minimum drop size accurately measured by the disdrometer is too large to characterize the fine diameters typical of drops landing close to the emitter. For further landing distances, the discrepancies between measurements and simulations using ballistic theory can be large. Differences in drop velocity, drop size and maximum sprinkler reach are discussed in the paper. From our results, it can be concluded that the ballistic model (assuming independent movement of drops) constitutes an excessive simplification of reality. We believe that group displacement of the drops, resulting in

a reduced air drag and in an increased probability of drop collision, is responsible for a relevant part of the reported differences.

Keywords: Disdrometer, drop, irrigation, sprinkler, ballistic model.

1 Introduction

Describing in detail the physics of sprinkler irrigation from the nozzle to the ground is not an easy task. In a first phase (usually 1 or 2 m downstream from the nozzle) drops travel as a jet, and therefore experience a reduced air drag (Seginer 1965). Kincaid (1996) proposed to reduce the drag coefficient in this initial phase. In a second phase, inertia and viscous forces break the jet from the outside towards the inside, yielding smaller drops with higher relative velocities (larger pressure) (von Bernuth and Gilley 1984; Seginer et al. 1991). In the final phase, along a transition zone, the jet completely disintegrates into drops which can be considered spherical and independent (von Bernuth and Gilley 1984). Along these three phases, drops are exposed to a probabilistic process of collisions. Additionally, drops larger than 5.5 mm in diameter are unstable and tend to break up into smaller droplets (Kincaid 1996).

Given the complexity of this process, simplified drop dynamics models (such as the ballistic model) are introduced for sprinkler irrigation simulation and design. The ballistic model (Seginer et al. 1991; Vories et al. 1987; Carrión et al. 2001; Playán et al. 2006) is based on the hypothesis that the drops are spherical and isolated. The aerodynamic resistance of an isolated drop has been accurately determined in the literature (Fukui et al. 1980; Seginer et al. 1991), leading to the establishment of the drop dynamics equations. These equations can be numerically solved using (for instance) a fourth order Runge-Kutta method.

Different methodologies have been reported in the literature to determine drop diameters resulting from precipitation, sprinkler irrigation or pesticide application. Montero et al. (2003) discussed a series of manual methods based on impression, photography, immersion in viscous fluids and impact on a layer of flour. These methods have been replaced by computer driven optical devices. Among them, optical methods using laser equipment (Kohl et al. 1985; Kincaid et al. 1996) and optical disdrometer methods (Salles and Poesen 1999; Montero et al. 2003).

Optical disdrometers measure the attenuation of an infrared beam when water drops pass across it, and have been extensively used to characterize drops resulting from precipitation (Bringi et al. 2006; Caracciolo et al. 2006; Lee and Zawadzki 2006). The beam section is circular in shape and centimetric in diameter. As a drop passes between the beam emitter and the detector, a decrease in electric potential is measured at the detector which is proportional to the drop shadow (Montero et al. 2003). The technique permits a measurement of drop size and drop velocity (time of passage) as the drop passes through a stationary detector. These variables are very relevant to the validation of sprinkler irrigation models. However, two experimental problems affect the quality of these measurements (Montero et al. 2003):

1. Several drops can overlap as they reach the disdrometer. In these circumstances the device will detect only one drop, with larger-than-real size and time of passage.

2. Drops can pass through a side of the detector, so that only part of the drop attenuates the luminous flow. As a consequence, the drop size and time of passage will be shorter-than-real.

These two problems can happen in a variety of cases, resulting in anomalous detections. A statistical analysis of different sources of error on the estimation of drop diameter was reported by Grossklaus et al. (1998). When disdrometers are used to evaluate sprinkler irrigation performance, they are located at soil level and moved along a radius stemming from an isolated sprinkler (Montero et al. 2003).

The current ballistic sprinkler simulation models rely on a number of semi-empirical and empirical parameters. The parameters of the statistical distribution of drop diameters emitted by the sprinkler can be input to the model, but in most practical applications are estimated during the calibration phase. Because of the experimental effort needed to calibrate and validate ballistic models, limited field applications have been reported in the literature (Montero et al. 2001; Playán et al. 2006). These applications included experiments with isolated sprinklers and solid-sets in outdoor and/or indoor conditions, over bare soils and with pluviometers located close to the soil level. Different combinations of sprinkler, nozzle and operation conditions were required. In the validation phase, the models showed adequate predictive capability even at sprinkler spacings and operating pressures different from the experimental ones. Calibration experiments have traditionally been performed over bare soil, although in practical applications the crop canopy grows with time. Even if the effects of canopy growth on wind profile and surface roughness are not accounted for, the increase in crop canopy elevation affects the drop landing distance by truncating drop trajectory. In these circumstances, the predictive capability of the model will decrease as the crop grows. Two alternative paths can be followed to solve this problem:

- calibrate the model using experiments at different crop heights; and
- reduce the model empiricism by measuring drop diameters and using the parameters of their statistical distribution to feed the model.

The second option is more rapid and cost effective, but faces problems related to data quality, as previously discussed.

In this work, we illustrate the experimental problems of using a disdrometer and demonstrate that a statistical treatment of the observed time of passage can be used to eliminate a large part of the erroneous measurements and to significantly improve the data accuracy. Pseudo-random drop sets are generated and used to simulate analytically the detector behavior and to assess the adequacy of the statistical data treatment methods. Finally, the optimum method is applied to a number of disdrometer data sets obtained under different sprinkler irrigation conditions at the Sprinkler Irrigation Laboratory of the University of Castilla-La Mancha (Albacete, Spain). The corrected data sets are compared to simulations performed with the ballistic model for validation purposes. Experimental data are also used to discuss the validity of the current ballistic models of sprinkler irrigation.

2 A ballistic model of sprinkler irrigation

The main hypothesis of this model is that the drops emitted by the sprinkler move as independent spheres in the surrounding air (Fukui et al. 1980; Carrión et al. 2001). The drag force of a sphere in turbulent flow can be expressed as:

$$\mathbf{F}_r = -\frac{1}{2}\lambda\rho_a A|\dot{\mathbf{r}} - \mathbf{w}|(\dot{\mathbf{r}} - \mathbf{w}) \tag{1}$$

where ρ_a is air density, A is the effective section, $\mathbf{r}$ is the position vector, $\mathbf{w}$ is the wind velocity vector, and λ is a drag coefficient depending on the Reynolds number. The ballistic dynamic equations of a drop constitute a set of three ordinary differential equations. In vector notation these equations can be expressed as:

$$m\ddot{\mathbf{r}} = -\frac{1}{2}\lambda\rho_a A|\dot{\mathbf{r}} - \mathbf{w}|(\dot{\mathbf{r}} - \mathbf{w}) + m\mathbf{g} \tag{2}$$

with m the drop mass and $\mathbf{g} = (0, 0, -g)^T$ the gravitatory field, with g the gravitational constant. Dividing this equation by the mass, and considering a spherical drop with diameter d:

$$\ddot{\mathbf{r}} = -\frac{3\lambda\rho_a}{4\rho_w d}|\dot{\mathbf{r}} - \mathbf{w}|(\dot{\mathbf{r}} - \mathbf{w}) + \mathbf{g} \tag{3}$$

with ρ_w the water density. λ can be approximated following (Fukui et al. 1980; Seginer et al. 1991) as:

$$\lambda = \begin{cases} 1.2 - 0.0033Re + 33.3/Re; & Re \in [0, 128) \\ 0.48 - 0.0000556Re + 72.2/Re; & Re \in [128, 1440) \\ 0.45; & Re \in [1440, \infty) \end{cases} \tag{4}$$

with $Re = d|\dot{\mathbf{r}}|/\nu$ the Reynolds number and ν the cinematic viscosity of the air. These equations are numerically solved using a fourth order Runge-Kutta method.

3 Statistical methods for drop data treatment

3.1 Basic hypotheses

Two hypotheses can be used to eliminate erroneous disdrometer drop measurements resulting from overlapping and side-passing drops.

- Drops of a given diameter reach the disdrometer at similar velocities. Consequently, a statistical treatment of time of passage should suffice to eliminate a relevant part of the erroneous measurements.

- The fall in electric potential at the infrared detector is proportional to the effective drop diameter. Since at the typical range of drop velocity in sprinkler irrigation drops can be considered spherical (Fukui et al. 1980), the drop shadow will be a circle with the same radius as the drop. If n drops characterized by diameters d_i overlap, we assume that the disdrometer detector will record diameter d_{det}, associated to the maximum possible detected shadow:

$$d_{det} = \max_t \sqrt{\sum_{i=1}^{n} d_i^2} \tag{5}$$

  As for the time of passage, we assume that it can be estimated as the elapsed time since the first drop enters the beam and the last drop exits from it. If a drop passes through the disdrometer beam laterally, the fall in electric potential will be proportional to the intersecting area between the effective drop section and the beam section.

Let's assume a detector with radius R (and diameter D), measuring a set of drops with uniform radius r (and diameter d) and uniform, vertical velocity with module v (fig. 1). We further assume that all of them reach the disdrometer with the same angle and that their trajectory can be considered linear inside the beam, given its relatively small size. We chose, for convenience, the axis z in the direction of drop movement. We also assume that the probability of drop arrival is independent of coordinate x. In these conditions, the time of passage of a drop at a coordinate x is:

$$T = \frac{2\sqrt{(R+r)^2 - x^2}}{v} \tag{6}$$

The average time of passage through the detector will be:

$$\overline{T} = \frac{\displaystyle\int_{-R-r}^{R+r} \frac{2\sqrt{(R+r)^2 - x^2}}{v} dx}{\displaystyle\int_{-R-r}^{R+r} dx} = \frac{\pi}{2}\frac{R+r}{v} \tag{7}$$

From the average time of passage, the drop velocity can be derived as:

$$v = \frac{\pi}{2}\frac{R+r}{\overline{T}} \tag{8}$$

The drops of a given diameter taking longer to pass through the detector are those travelling across the center of the circle. The time of passage for these drops will be:

$$T_{max} = \frac{2(R+r)}{v} \tag{9}$$

Consequently, the ratio between the maximum and average times of passage will be:

$$\frac{T_{max}}{\overline{T}} = \frac{4}{\pi} \tag{10}$$

If the detector records a time of passage $T > T_{max}$, the drops must have overlapped and as a consequence the record can be considered incorrect.

In the system of reference with origin in the center of the detector and axis z in the direction of drop movement, drops will laterally pass through the detector if $x \in (-R-r, -R+r) \cup (R-r, R+r)$. In these cases, the time of passage will satisfy the condition:

$$T < T_{min} = \frac{2\sqrt{(R+r)^2 - (R-r)^2}}{v} = \frac{4}{v}\sqrt{Rr} \tag{11}$$

The ratio between the minimum time and the average recorded time is:

$$\frac{T_{min}}{\overline{T}} = \frac{8}{\pi}\frac{\sqrt{Rr}}{R+r} \tag{12}$$

It can be assumed that it the detector records a time of passage $T < T_{min}$, the drop has laterally passed through the detector and as a consequence the record can also be considered incorrect.

3.2 Initial method for erroneous drop removal

Figure 2 presents the flow diagram of the algorithm used to remove erroneous drop records based on a statistical treatment of the time of passage. Criteria (10) and (12) have been applied with tolerance τ, which reflects a certain variability in drop velocity.

3.3 Improved method for erroneous drop removal

Figure 3 presents an improved version of the algorithm, based on an initial tolerance of 0.2. The tolerance is iteratively relaxed by 0.1 increments, if the removed drops reach 90%. This tolerance relaxation is supported by the tests developed in the following section.

4 Theoretical tests: pseudo-random generation of a set of drops

Let's define two average parameters associated to the drop size of a set of n drops with diameters d_i. The first parameter is the numerical average, defined as:

$$d^n = \frac{\sum_{i=1}^{n} d_i}{n} \tag{13}$$

The second parameter is the volumetric average, defined as:

$$d^v = \frac{\sum_{i=1}^{n} d_i \frac{1}{6}\pi d_i^3}{\sum_{i=1}^{n} \frac{1}{6}\pi d_i^3} \tag{14}$$

This analysis can also be applied to the times of passage, yielding:

$$T^n = \frac{\sum_{i=1}^{n} T_i}{n}, \qquad T^v = \frac{\sum_{i=1}^{n} T_i \frac{1}{6}\pi d_i^3}{\sum_{i=1}^{n} \frac{1}{6}\pi d_i^3} \tag{15}$$

In order to test the effectiveness of the proposed statistical method, a pseudo-random drop set can be generated following a triangular probability law:

$$p(d) = \begin{cases} 0; & (d \leq d_{min},\ d \geq d_{max}) \\ 2\frac{d-d_{min}}{(d_{mean}-d_{min})(d_{max}-d_{min})}; & (d_{min} < d < d_{mean}) \\ 2\frac{d_{max}-d}{(d_{max}-d_{mean})(d_{max}-d_{min})}; & (d_{mean} \leq d < d_{max}) \end{cases} \tag{16}$$

For a given pseudo-random number $x \in [0, 1)$, the drop diameter can be generated as follows:

$$d = \begin{cases} d_{min} + \sqrt{x(d_{max} - d_{min})(d_{mean} - d_{min})}; & \left(x \leq \frac{d_{mean}-d_{min}}{d_{max}-d_{min}}\right) \\ d_{max} - \sqrt{(1-x)(d_{max} - d_{min})(d_{max} - d_{mean})}; & \left(x > \frac{d_{mean}-d_{min}}{d_{max}-d_{min}}\right) \end{cases} \tag{17}$$

Triangular probability was chosen for the test cases for conceptual simplicity and because it allows for adequate visual appreciation of the differences in the density function following drop removal.

With the center of the detector located at the origin of coordinates (fig. 1), a region of drops was created with the following bounds: $x \in [-R - r_{max}, R + r_{max}]$, $y \in [R + r_{max}, R + r_{max} + L]$. In this region, the centers of N drops were pseudo-randomly generated with uniform probability. In the course of each numerical test, all generated drops move vertically downwards, simulating a pass through the detector.

The relative drop density, σ, expresses the average number of drops passing through the detector. It is computed dividing the total number of drops by the ratio of the areas of the region of drops and the detector:

$$\sigma = \frac{N}{\frac{2(R+r_{max})L}{\pi R^2}} \tag{18}$$

The higher the value of σ the higher the probability of drop overlap when passing through the disdrometer beam.

Two sets of drops, with 200000 elements each, were generated for the purpose of assessing the statistical drop removal method. The sets differ in the hypothesis for drop velocity:

Test 1: Uniform drop velocity. In this case, all drops have uniform velocity. This assumption is coincident with the main hypothesis of the proposed method: all drops reach the disdrometer with similar velocity. As a consequence, this should be an optimum case for the method. The drop size fluctuates between $d_{min} = 1$ mm and $d_{max} = 8$ mm, with $d_{mean} = 4$ mm. Drop velocity equals $v = 1$ m/s. The detector diameter is $D = 20$ mm.

Test 2: Drops with variable, random velocity. Each drop in the set has a pseudo-random velocity ranging between 1 and 2 m/s, with uniform probability. The rest of the parameters are as in Test 1.

Figure 4 presents the errors incurred in the estimation of the numerical and volumetric average diameters with the unprocessed simulated disdrometer and applying the initial method with different tolerances. Figure 5 presents the corresponding errors for the numerical and volumetric average times of passage. The results are strongly dependent on the drop density σ, but the introduction of a variable drop velocity does not have a relevant impact on the quality of the results. The tolerance parameter does have an important effect on the results: in general, for low values of σ, accurate results are obtained when the tolerance is low. However, for large values of σ and low tolerance, the method can eliminate an excessive number of drops, favoring small drop diameters. The same can be observed when tolerances are very small: tolerances below 0.2 do not improve the quality of the results and eliminate an excessive number of drops. Errors are much larger for the time of passage than for the drop diameter. The need for the proposed statistical method is therefore more evident for the time than for the diameter.

Figures 6 and 7 present the errors in diameter and time respectively as a function of drop removal. In all cases errors increase with drop removal, and accuracy increases as tolerance decreases. When more than about 90% of the drops are removed, small drops are largely favored and errors become strongly negative. In these cases, it is an adequate strategy to increase tolerance, resulting in an increase in the ratio of remaining drops and a reduced error. These observations led to the formulation of the improved method for erroneous drop removal.

Figure 8 presents a histogram of drop diameter as registered by the disdrometer and as corrected using the improved method. Both histograms are compared with the real, triangular frequency distribution used in the numerical tests. For low relative drop densities ($\sigma = 0.1$) the corrected histogram is very similar to the real histogram. In this case, the errors evidenced at the right and left sides of the distribution of figure 8-a, due to overlapping and side-passing drops, respectively, are almost completely corrected (fig. 8-b). As a result, the resulting distribution shows only minor differences with the real distribution. The improvements introduced by the rejection of erroneous drops are quantitatively much more relevant for high relative drop densities ($\sigma = 1$). Under these circumstances, the detector reflects a high percentage of larger-than-real drop diameters. Introducing variability in drop velocity (test 2) moderates the improvements resulting from the use of the method. The corrected results are, however, much closer to the real distribution than the detected results.

5 Experimental tests: disdrometer and sprinkler

The proposed methodology is applied in this section to disdrometer measurements performed at the Sprinkler Irrigation Laboratory of the University of Castilla-La Mancha (Albacete, Spain). The tested sprinkler was a VYR35 manufactured by VYRSA (Burgos, Spain). The operating pressures were 200, 300 and 500 kPa. The sprinkler was equipped with principal nozzles of 3.2, 4.8 and 6.0 mm in diameter. Auxiliary nozzles were not used in the experiments. The vertical Emission angle of the sprinkler is 25°. The sprinkler nozzle was located at an elevation of 0.6 m from the soil surface. The optical disdrometer model used in this research was ODM 470, manufactured by Eigenbrodt (Königsmoor, Germany). The specifications and configuration of the optical disdrometer were as reported by Montero et al. (2006). The minimum drop size accurately measured by the disdrometer is 0.5 mm. The detector was located in a radial pit (with the sprinkler on one side) at an elevation of -0.23 m from soil surface elevation. Measurements were performed locating the disdrometer at distances from the sprinkler multiple of 3 m to a distance of 15 m. Two series of experiments were performed:

- with the sprinkler head fixed to prevent it from rotating; and
- with the sprinkler head rotating freely.

Table 1 presents the maximum reach of the sprinkler in each experiment, as detected with the pluviometers. The results reveal a relevant difference between both experimental series (from 1.2 to 2.4 m), in favor of the fixed sprinkler head. This difference is positively correlated with the operating pressure, and can not be attributed to ballistics.

Given the high initial drop velocity (20-30 m/s), the difference can not be attributed to mechanical effects related to the rotating velocity of the sprinkler head (orders of magnitude lower than that the initial drop velocity). This effect was reported previously by Bilanski and Kidder (1958) and Seginer (1963), and was attributed by Seginer et al. (1991) to the reduced drag experienced by a jet section or a drop moving along the unchanging trajectory resulting from a fixed sprinkler head. In fact, the fixed sprinkler creates a stream of air around the drop jet which moves along it. As a consequence, in a fixed sprinkler the relative drop velocity and the resulting drag coefficient are smaller than if the air was completely still, as assumed by the ballistic model in this case. The difference in reach between both series of experiments constitutes a relevant evidence that:

- the effect of the group displacement of the drops (resulting in a reduced air drag and in an increased probability of drop collision) is relevant; and
- that the ballistic model (assuming independent movement of drops) constitutes an excessive simplification of reality.

The improved method for erroneous drop removal was always used with a tolerance of 0.2. As presented in figure 9, the percentage of removed drops in the experimental runs fluctuated between 15 and 70%, with most of the cases showing a removal of about 30% of the drops. Using this tolerance, and extrapolating from tests 1 and 2, the magnitude of the measurement error for drop diameter would be lower than 10%, while the error for time of passage would be lower than 30%. The figure also shows that fixing the sprinkler head and aiming it at the disdrometer results in a significant increase in the number of drops passing through the detector.

Figure 10 presents the drop trajectories obtained with the ballistic simulation model for the experimental conditions. Following Kincaid (1996), simulation results are also presented for a situation in which no aerodynamic resistance was considered in the first meter of the trajectory. In this distance the jet is compact, and is not broken down in drops. In all cases, the trajectory is presented for the drop diameter landing at the points where the disdrometer was located. In the area near the sprinkler ($\leq$ 3 m), the drop size is lower than the minimum drop size accurately measured by the disdrometer (0.5 mm). Figure 11 presents for the same cases the relationship between the drop velocity and the distance to the sprinkler.

Figure 12 presents the percentage of emitted water volume as a function of drop diameter as measured with the disdrometer and as treated with the improved method for erroneous drop removal. These data are compared with the simulated drop diameters resulting in trajectories reaching the ground at the location of the disdrometer. These diameters are presented for a full drop trajectory (right) and for a 1 m compact jet before breaking out into drops (left). In all presented cases, the ballistic drop diameters exceed the detection limit of the device.

Tables 2 and 3 present different drop diameters simulated, measured and corrected with the improved method. Diameters d_{20}, d_{50} and d_{80} represent the diameters corresponding to 20%, 50% and 80%, respectively, of the volume of detected water. Both tables present the results of the complete experimental data set. The tables confirm that the disdrometer only rarely measured drops smaller than 1 mm. After the proposed correction, the fraction of drops with diameter over 6 mm is close to null in most cases. According to Kincaid (1996), this diameter is unstable and breaks up into smaller drops. The tables permit comparation of all three sources of diameter data with a variety of parameters, including the statistical distribution of measured and corrected drop diameters. The average values presented at the end of both tables reflect the improvements in diameter estimation in terms of d_{max} (approaching realistic values) and in terms of d_{50} (as compared to the ballistic estimates). To further support this last point, figure 13 presents two scatter plots confronting the simulated diameters (with and without the 1 m jet) with the corrected values of d_{50}. The scatter plot places most points in the vicinity of the 1:1 solid line, denoting a reasonable agreement.

One of the most interesting results of the experiments is that even after treatment, the disdrometer indicates that a wide range of drop diameters is collected at each measurement location. This finding is not compatible with the ballistic theory, which indicates that for a given no-wind experiment the drop landing distance is only a function of drop diameter. As a consequence, drops of very similar diameters should be registered at each measurement location. Three possible explanations seem feasible for this phenomenon:

- Since the drops travel in groups after the break-up of the jet, their aerodynamic resistance is reduced. If this effect was relevant, the measured drop size should be slightly smaller than predicted by the model. On the other hand, large drops abandoning the group early could experiment similar drag than fine drops. Consequently the drop diameter at a given location should be somewhat heterogeneous.

- If drops move in compact groups during a large part of their trajectory, there is a significant probability of collisions between drops, resulting in fusions. This could explain the presence of drops considerably larger than expected. Neither ballistics nor the reduced air drag resulting from the existence of groups of drops can explain the existence of these drops. Collisions could also result in the formation of smaller drops. This effect could partially explain the heterogeneity in drop sizes.

- In the process of jet break-up large drops, exceeding 6 mm in diameter, are formed. These unstable drops end up breaking up into smaller droplets during their trajectory. This could explain the measurement of large drops (with d_{80} occasionally exceeding 7 mm) and the measurement of small drops far away from the sprinkler.

Finally, figure 14 presents a comparison between the final drop velocities as simulated with the ballistic model (using a full drop trajectory and a 1 m compact jet before breaking out into drops) and as measured with the disdrometer (with a rotating and a fixed sprinkler head). Results are displayed for the different distances to the sprinkler. In the case of the ballistic data, velocities are presented for the drop size diameter at the observation point. In the case of the experimental data, results are presented for the nozzle(s) used in the experiment(s) (between one and three). Different trends can be observed in the velocity estimates resulting from disdrometer time of passage (velocity decreases with distance) and from ballistic simulations (velocity increases with distance). Although a reasonable agreement can be observed at a distance of about 15 m from the sprinkler, there is a remarkable difference in velocities at other distances, closer to the sprinkler. This difference is larger than the 30% accuracy that could be expected according to the disdrometer accuracy determined from numerical tests. Even if the disdrometer accuracy for velocity determinations is only fair, the differences observed in the figure add to the discussions about the validity of the ballistic model for the reported conditions.

6 Conclusions

In this work, we have shown how a statistical treatment of the times of passage measured with an optical disdrometer can eliminate a large number of erroneous measurements. These measurement errors can be due either to the simultaneous or to the lateral passage of drops. The treatment has largely improved the accuracy in the estimation of drop diameters. The times of passage also permit to estimate drop velocity. The theoretical analysis has shown that the error in the estimation of velocity is significantly larger than the error in the estimation of diameter. However, the proposed statistical treatment can improve the quality of the results and permits to obtain reasonable estimates of drop velocity.

For the usual sprinkler irrigation operating pressures, the ballistic model predicts drop diameters in the range of 0.5-0.7 mm at a distance of 3 m from the sprinkler. These drop diameters are too close to the minimum drop diameter detected by the disdrometer (about 0.5 mm) to ensure accurate results. As a consequence, the disdrometer should only be used at larger distances ($\geq$ 6 m) from the sprinkler. A reduction in the lower limit of drop diameter detection would permit accurate disdrometric measurements closer to the sprinkler.

Drop measurements and their statistical treatments in a series of experiments performed in a laboratory at sufficiently large distances from the sprinkler have revealed relevant discrepancies that cast shadows over the validity of the current ballistic models. The experiments have revealed that:

- there is a notable discrepancy between simulated and measured drop velocity;

- there is a large variability in drop diameter at a given location from the sprinkler;

and

- there is a substantial increase (1.2-2.4 m) in the maximum sprinkler reach when the sprinkler head is fixed to prevent rotation. These results confirm previous reports.

In addition to these findings, which can not be explained by ballistics, the model needs empirical calibration in the presence of wind (Tarjuelo et al. 1994; Carrión et al. 2001). Two additional parameters (denoted K_1 and K_2) must be calibrated for each combination of sprinkler, operating pressure, nozzle diameter and for a range of wind speeds. We are under the impression that the reason for all these discrepancies is the fact that the movement of drops in groups results in a relevant effect on:

- the reduction of the aerodynamic drag; and
- an increase of the probability of drop collisions resulting in new drop diameters.

Current sprinkler irrigation ballistic models do not consider such processes. As a consequence, a model review seems required to produce reliable, empiricism-free model results.

References

Bilanski, W. K. and E. H. Kidder (1958). Factors that affect the distribution of water from a medium-pressure rotary irrigation sprinkler. *Trans. of the ASAE 1*(1), 19–28.

Bringi, V. N., M. Thurai, K. Nakagawa, G. J. Huang, , T. Kobayashi, and A. Adachi (2006). Rainfall estimation from C-band polarimetric radar in Okinawa, Japan: comparisons with 2D-video disdrometer and 400 MHz wind profiler. *J. the Meteorological Soc. of Japan 84*(4), 705–724.

Caracciolo, C., F. Prodi, and R. Uijlenhoet (2006). Comparison between Pludix and impact/optical disdrometers during rainfall measurement campaigns. *Atmospheric Res. 82*(1–2), 137–163.

Carrión, P., J. M. Tarjuelo, and J. Montero (2001). SIRIAS: a simulation model for sprinkler irrigation I: description of model. *Irrig. Sci. 20*, 73–84.

Fukui, Y., K. Nakanishi, and S. Okamura (1980). Computer evaluation of sprinkler irrigation uniformity. *Irrig. Sci. 2*, 23–32.

Grossklaus, M., K. Uhlig, and L. Hasse (1998). An optical disdrometer for use in high wind speeds. *J. Atmospheric and Oceanic Tech. 15*, 1051–1059.

Kincaid, D. C. (1996). Spraydrop kinetic energy from irrigation sprinklers. *Trans. of the ASAE 39*, 847–853.

Kincaid, D. C., K. H. Solomon, and J. C. Oliphant (1996). Drop size distributions for irrigation sprinklers. *Trans. of the ASAE 39*(3), 839–845.

Kohl, R. A., R. D. von Bernuth, and G. Heubner (1985). Drop size distribution measurement problems using a laser unit. *Trans. of the ASAE 28*(1), 190–192.

Lee, G. and I. Zawadzki (2006). Radar calibration by gage, disdrometer, and polarimetry: theoretical limit caused by the variability of drop size distribution and application to fast scanning operational radar data. *J. Hydrology 328*(1–2), 83–97.

Montero, J., P. Carrión, J. M. Tarjuelo, and R. A. Nin (2006). Calibración de un disdrómetro óptico para la medida de tamaños de gota producidos por los aspersores. *XXIV Congreso Nacional de Riegos*, Lugo, Spain.

Montero, J., J. M. Tarjuelo, and P. Carrión (2001). SIRIAS: a simulation model for sprinkler irrigation II: calibration and validation of the model. *Irrig. Sci. 20*(2), 85–98.

Montero, J., J. M. Tarjuelo, and P. Carrión (2003). Sprinkler droplet size distribution measured with an optical spectropluviometer. *Irrig. Sci. 22*(2), 47–56.

Playán, E., N. Zapata, J. M. Faci, D. Tolosa, J. L. Lacueva, J. Pelegrín, R. Salvador, I. Sánchez, and A. Lafita (2006). Assessing sprinkler irrigation uniformity using a ballistic simulation model. *Agric. Water Mgmt. 84*(1–2), 89–100.

Salles, C. and J. Poesen (1999). Perfomance of an optical spectro pluviometer in measuring basic rain erosivity characteristics. *J. Hydrology 218*(3–4), 142–156.

Seginer, I. (1963). Water distribution from medium pressure sprinklers. *ASCE J. the Irrig. and Drainage Div. 89*(2), 13–30.

Seginer, I. (1965). Tangential velocity of sprinkler drops. *Trans. of the ASAE 8*, 90–93.

Seginer, I., D. Nir, and R. D. von Bernuth (1991). Simulation of wind-distorted sprinkler patterns. *J. Irrig. and Drainage Eng. 117*, 285–305.

Tarjuelo, J. M., P. Carrión, and M. Vicente (1994). Simulación de la distribución del riego por aspersión en condiciones de viento. *Investigación Agraria. Producción y Protección Vegetal 9*, 255–272.

von Bernuth, R. D. and J. R. Gilley (1984). Sprinkler drop size distribution estimation from single leg test data. *Trans. of the ASAE 27*, 1435–1441.

Vories, E. D., R. D. von Bernuth, and R. H. Mickelson (1987). Simulating sprinkler performance in wind. *J. Irrig. and Drainage Eng. 113*, 119–130.

Nomenclature

A = effective drop section area.

D = detector diameter.

d = drop diameter.

d_{20}, d_{50}, d_{80} = diameters corresponding to 20%, 50% and 80%, respectively, of the volume of detected water.

d_{det} = detected drop diameter.

$\mathbf{F}_r$ = drag force.

$\mathbf{g}$ = gravitatory field.

g = gravitational constant.

K_1, K_2 = empirical wind effect parameters of the ballistic model.

L = height of the drop pseudo-random generation region.

m = drop mass.

P = sprinkler pressure.

p = probability.

R = detector radius.

$\mathbf{r}$ = vector of drop position.

r = drop radius.

Re = Reynolds number.

T = drop passage time.

$\overline{T}$ = average drop passage.

t = time.

T_{max} = maximum passage time.

T_{min} = minimum passage time.

v = velocity module.

$\mathbf{w}$ = wind velocity.

x, y, z = spatial coordinates.

λ = drag coefficient.

ν = cinematic viscosity of the air.

ρ_a = air density.

ρ_w = drop density.

σ = relative drop density.

τ = tolerance.

ϕ = sprinkler nozzle diameter.

List of Tables

1 Maximum sprinkler reach for different operating pressures and nozzle diameters with a (a) rotating and (b) fixed sprinkler head. 25

2 Different estimations of drop diameter for the experiments performed with a rotating sprinkler head. Simulated estimations using the ballistic model include d_I (with an initial 1 m jet) and d_{II} (without jet). Measured and corrected (rejecting drops) estimations are presented for d_{min}, d_{max} and for d_{20}, d_{50} and d_{80} (representing the diameters corresponding to 20%, 50% and 80%, respectively, of the volume of detected water). The experiments are coded following a convention for nozzle diameter (A: 3.2 mm, B: 4.8 mm and C: 6.0 mm), operating pressure (a: 200 kPa, b: 300 kPa y c: 500 kPa) and distance from the sprinkler to the detector (1: 6 m, 2: 9 m, 3: 12 m y 4:15 m). Average values are presented in the last row. 26

3 Different estimations of drop diameter for the experiments performed with a fixed sprinkler head. Simulated estimations using the ballistic model include d_I (with an initial 1 m jet) and d_{II} (without jet). Measured and corrected (rejecting drops) estimations are presented for d_{min}, d_{max} and for d_{20}, d_{50} and d_{80} (representing the diameters corresponding to 20%, 50% and 80%, respectively, of the volume of detected water). The experiments are coded following a convention for nozzle diameter (A: 3.2 mm, B: 4.8 mm and C: 6.0 mm), operating pressure (a: 200 kPa, b: 300 kPa y c: 500 kPa) and distance from the sprinkler to the detector (1: 6 m, 2: 9 m, 3: 12 m y 4:15 m). Average values are presented in the last row. 27

List of Figures

1 Representation of a drop of radius r passing across a disdrometer detector with radius R 28

2 Flow diagram for the initial method for erroneous drop removal 29

3 Flow diagram for the improved method for erroneous drop removal . . . 30

4 Percent error in the estimation of average diameter (a) and (c) volumetric, (b) and (d) numerical, as a function of σ for the unprocessed simulated disdrometer reading and for the proposed initial method for erroneous drop removal with different tolerances and for tests (a) and (b) 1, (c) and (d) 2. 31

5 Percent error in the estimation of average time of passage (a) and (c) volumetric, (b) and (d) numerical, as a function of σ for the unprocessed simulated disdrometer reading and for the proposed initial method for erroneous drop removal with different tolerances and for tests (a) and (b) 1, (c) and (d) 2. 32

6 Percent error in the estimation of average diameter (a) and (c) volumetric, (b) and (d) numerical, as a function of the percentage of rejected drops for the unprocessed simulated disdrometer reading and for the proposed initial method for erroneous drop removal with different tolerances and for tests (a) and (b) 1, (c) and (d) 2. 33

7 Percent error in the estimation of average time of passage (a) and (c) volumetric, (b) and (d) numerical, as a function of the percentage of rejected drops for the unprocessed simulated disdrometer reading and for the proposed initial method for erroneous drop removal with different tolerances and for tests (a) and (b) 1, (c) and (d) 2. 34

8 Histogram of drop diameter as detected by the disdrometer (a), (c) and (e), and as corrected using the improved method for drop rejection (b), (d) and (f). The relative drop density, σ, was 0.1 in (a) and (b), and 1 in (c), (d), (e) and (f). Test 1 (uniform drop velocity) was run in (a), (b), (c) and (d), while Test 2 (variable, random drop velocity) was run in (e) and (f). In all cases experimental histograms are compared with the real, triangular frequency distribution used in the numerical tests. 35

9 Percentage of drop removal with the improved method as a function of total number of detected drops for rotating and fixed sprinkler head. . . . 36

10 Simulated drop trajectories for pressures of (a) and (b) 200, (c) and (d) 300, (e) and (f) 500 kPa. In (b), (d) and (f) aerodynamic resistance was assumed zero for the first 1 m of the jet. 37

11 Simulated drop velocities for pressures of (a) and (b) 200, (c) and (d) 300, (e) and (f) 500 kPa. In (b), (d) and (f) aerodynamic resistance was assumed zero for the first 1 m of the jet. 38

12 Percentage of emitted water volume as a function of drop diameter as measured with the disdrometer and as treated with the improved method for erroneous drop removal. These data are compared with the simulated drop diameters resulting in trajectories reaching the ground at the location of the disdrometer. These diameters are presented for a full drop trajectory (right) and for a 1 m compact jet before breaking out into drops (left). Results are presented for an operating pressure, for a distance to the sprinkler and for nozzle diameters of (a) 200 kPa, 6 m, 4.8 mm, (b) 300 kPa, 6 m, 6.0 mm, (c) 500 kPa, 9 m, 3.2 mm, (d) 200 kPa, 9 m, 4.8 mm, (b) 300 kPa, 12 m, 6.0 mm, (c) 500 kPa, 15 m, 3.2 mm. Sprinkler head rotated in (a), (c) and (e), and was fixed in (b), (d) and (f). . 39

13 Simulated drop diameters ((a) without jet, (b) with a 1 m jet) vs. average corrected drop diameters (d_{50}) at different distances from the sprinkler. Results are presented for the whole experimental set, noting the experiments performed with fixed and rotating sprinkler head. The lines included in both plots have a 1:1 slope. 40

14 Final drop velocities as simulated with the ballistic model for the drop diameter landing at the observation point (using a full drop trajectory and a $1m$ compact jet before breaking out into drops) and (a), (c) and (e) as measured with the disdrometer (for the nozzles used in the experiments with a rotating and a fixed sprinkler head), (b), (d) and (f) using the improved method for erroneous drop removal. Results are displayed for the different distances to the sprinkler and for pressures of (a) and (b) 200, (c) and (d) 300, and (e) and (f) 500 kPa. 41

Table 1: Maximum sprinkler reach for different operating pressures and nozzle diameters with a (a) rotating and (b) fixed sprinkler head.

$\phi \backslash P$	200 kPa		300 kPa		500 kPa	
	a	b	a	b	a	b
3.2mm	12.6m	13.8m	-	-	14.4m	16.8m
4.8mm	14.4m	15.6m	16.2m	18m	-	-
6.0mm	14.4m	15.6m	16.2m	18m	-	-

Table 2: Different estimations of drop diameter for the experiments performed with a rotating sprinkler head. Simulated estimations using the ballistic model include d_I (with an initial 1 m jet) and d_{II} (without jet). Measured and corrected (rejecting drops) estimations are presented for d_{min}, d_{max} and for d_{20}, d_{50} and d_{80} (representing the diameters corresponding to 20%, 50% and 80%, respectively, of the volume of detected water). The experiments are coded following a convention for nozzle diameter (A: 3.2 mm, B: 4.8 mm and C: 6.0 mm), operating pressure (a: 200 kPa, b: 300 kPa y c: 500 kPa) and distance from the sprinkler to the detector (1: 6 m, 2: 9 m, 3: 12 m y 4:15 m). Average values are presented in the last row.

	Simulated		Measured					Rejecting drops				
	d_I mm	d_{II} mm	d_{min} mm	d_{20} mm	d_{50} mm	d_{80} mm	d_{max} mm	d_{min} mm	d_{20} mm	d_{50} mm	d_{80} mm	d_{max} mm
Aa1	1.14	1.41	1.12	1.77	2.23	3.12	7.21	1.12	1.64	1.88	2.23	3.12
Ba1	1.14	1.41	1.02	1.66	2.10	2.60	3.67	1.02	1.49	1.81	2.12	2.78
Ca1	1.14	1.41	1.19	1.95	2.36	2.75	3.53	1.19	1.84	2.23	2.59	3.44
Bb1	1.03	1.25	1.03	1.51	1.82	2.27	3.29	1.03	1.41	1.65	1.92	2.63
Cb1	1.03	1.25	1.11	1.58	1.93	2.31	3.70	1.11	1.54	1.80	2.09	2.70
Ac1	0.92	1.10	1.17	1.55	1.74	1.98	2.59	1.17	1.51	1.66	1.87	2.41
Aa2	1.97	2.39	1.18	3.42	4.41	4.93	10.03	1.18	3.02	3.67	4.22	4.93
Ba2	1.97	2.39	0.94	1.88	2.56	3.62	6.25	0.94	1.65	2.06	2.94	3.70
Ca2	1.97	2.39	1.12	2.61	3.79	4.93	5.90	1.12	1.88	2.63	3.41	4.99
Bb2	1.69	2.00	1.12	1.69	2.24	3.04	4.43	1.12	1.52	1.83	2.39	3.86
Cb2	1.69	2.00	1.12	1.84	2.46	3.17	5.05	1.12	1.68	2.11	2.84	5.05
Ac2	1.47	1.70	1.16	1.76	2.11	2.62	3.61	1.17	1.70	1.98	2.45	3.13
Ba3	3.26	3.89	0.95	3.29	4.57	5.75	6.99	0.95	3.02	4.59	5.11	6.02
Ca3	3.26	3.89	0.93	5.58	7.88	8.70	15.56	0.93	4.32	5.47	6.15	6.95
Bb3	2.59	3.02	1.04	2.68	3.99	5.39	8.36	1.04	2.27	3.17	4.24	6.50
Cb3	2.59	3.02	1.10	4.63	9.53	9.53	15.69	1.10	2.41	3.51	5.17	5.98
Ac3	2.14	2.43	1.26	2.56	3.35	4.74	6.70	1.27	2.29	2.93	3.97	4.74
Bb4	5.18	6.03	1.05	3.84	4.89	5.44	6.59	1.05	3.45	4.53	5.10	5.77
Avg	2.01	2.39	1.09	2.54	3.55	4.27	6.62	1.09	2.15	2.75	3.38	4.37

Table 3: Different estimations of drop diameter for the experiments performed with a fixed sprinkler head. Simulated estimations using the ballistic model include d_I (with an initial 1 m jet) and d_{II} (without jet). Measured and corrected (rejecting drops) estimations are presented for d_{min}, d_{max} and for d_{20}, d_{50} and d_{80} (representing the diameters corresponding to 20%, 50% and 80%, respectively, of the volume of detected water). The experiments are coded following a convention for nozzle diameter (A: 3.2 mm, B: 4.8 mm and C: 6.0 mm), operating pressure (a: 200 kPa, b: 300 kPa y c: 500 kPa) and distance from the sprinkler to the detector (1: 6 m, 2: 9 m, 3: 12 m y 4:15 m). Average values are presented in the last row.

	Simulated		Measured					Rejecting drops				
	d_I mm	d_{II} mm	d_{min} mm	d_{20} mm	d_{50} mm	d_{80} mm	d_{max} mm	d_{min} mm	d_{20} mm	d_{50} mm	d_{80} mm	d_{max} mm
Aa1	1.14	1.41	1.16	1.66	1.84	2.06	2.82	1.16	1.62	1.78	1.92	2.50
Ba1	1.14	1.41	1.26	1.78	2.02	2.34	3.40	1.26	1.75	1.98	2.30	3.40
Ca1	1.14	1.41	1.15	1.65	1.90	2.24	3.29	1.15	1.60	1.82	2.11	3.29
Bb1	1.03	1.25	1.40	1.76	1.97	2.22	3.03	1.40	1.75	1.94	2.17	2.84
Cb1	1.03	1.25	0.99	1.51	1.77	2.11	3.09	0.99	1.41	1.62	1.82	2.53
Ac1	0.92	1.10	1.21	1.52	1.68	1.87	2.29	1.21	1.50	1.65	1.80	2.22
Aa2	1.97	2.39	1.34	2.22	2.80	3.55	7.67	1.34	1.96	2.35	2.76	3.99
Ba2	1.97	2.39	1.34	2.11	2.62	3.36	7.69	1.39	1.95	2.28	2.75	3.86
Ca2	1.97	2.39	1.11	2.27	2.90	3.72	8.51	1.11	1.97	2.41	2.95	4.82
Bb2	1.69	2.00	1.39	2.04	2.37	2.81	4.99	1.39	1.95	2.22	2.58	3.47
Cb2	1.69	2.00	1.04	2.13	2.78	3.53	6.43	1.04	1.68	2.06	2.49	3.79
Ac2	1.47	1.70	1.26	1.71	1.93	2.20	3.63	1.26	1.65	1.82	2.02	2.91
Aa3	3.26	3.89	1.18	3.81	4.99	7.65	10.71	1.18	3.08	4.11	5.13	7.07
Ba3	3.26	3.89	1.42	3.02	4.19	6.10	10.75	1.42	2.36	2.97	3.97	5.85
Ca3	3.26	3.89	1.30	4.15	5.44	7.28	13.39	1.30	3.47	4.92	5.89	8.58
Bb3	2.59	3.02	1.39	2.37	3.01	4.12	8.43	1.39	2.11	2.52	3.10	6.36
Cb3	2.59	3.02	0.97	2.68	3.84	5.73	10.27	0.97	1.83	2.67	3.65	5.60
Ac3	2.14	2.43	1.12	1.92	2.29	2.74	4.51	1.12	1.76	2.00	2.27	3.21
Ba4	5.18	6.03	1.33	4.84	6.33	8.31	11.33	1.33	4.28	5.40	6.59	9.41
Ca4	5.18	6.03	1.16	6.61	8.77	13.32	16.06	1.18	5.34	6.57	7.57	9.09
Bb4	3.82	4.35	1.25	3.18	4.16	6.87	9.97	1.25	2.57	3.40	4.20	5.36
Cb4	3.82	4.35	1.09	3.60	5.01	7.97	11.46	1.09	3.00	4.25	5.96	11.33
Ac4	2.96	3.34	1.16	2.66	3.17	3.92	6.60	1.16	2.54	3.01	3.50	4.88
Avg	2.40	2.82	1.22	2.66	3.38	4.61	7.41	1.22	2.31	2.86	3.46	5.06

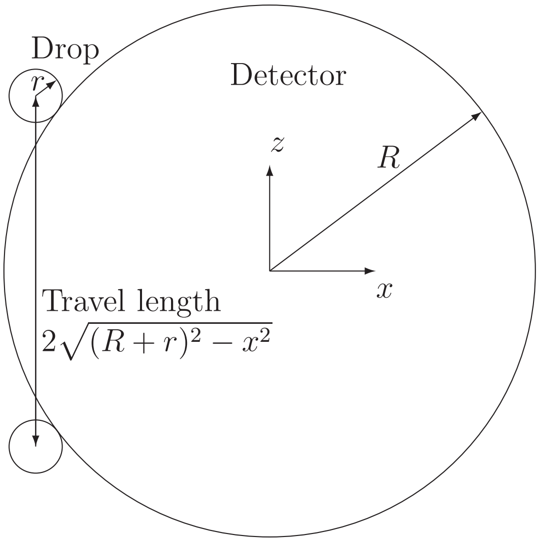

Figure 1: Representation of a drop of radius r passing across a disdrometer detector with radius R

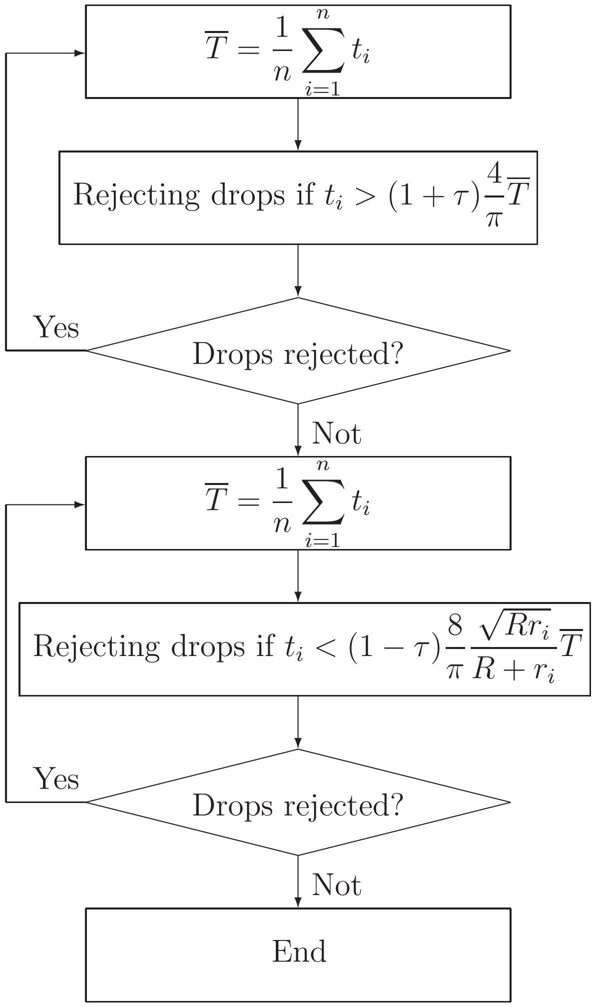

Figure 2: Flow diagram for the initial method for erroneous drop removal

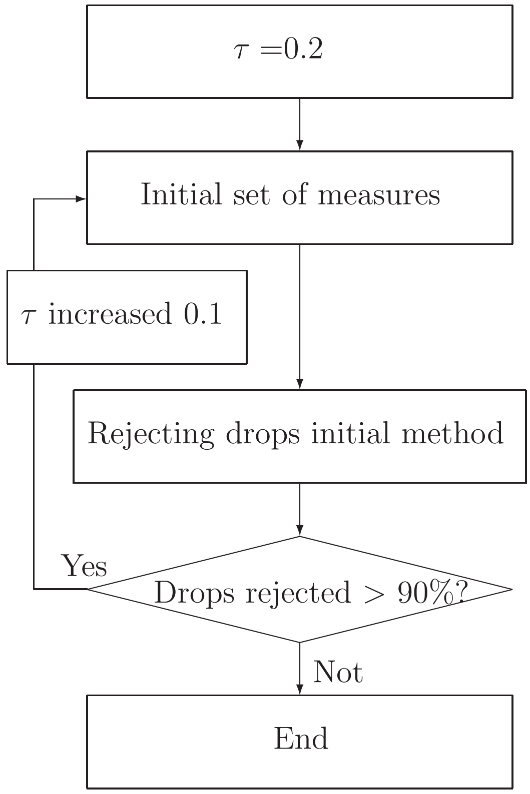

Figure 3: Flow diagram for the improved method for erroneous drop removal

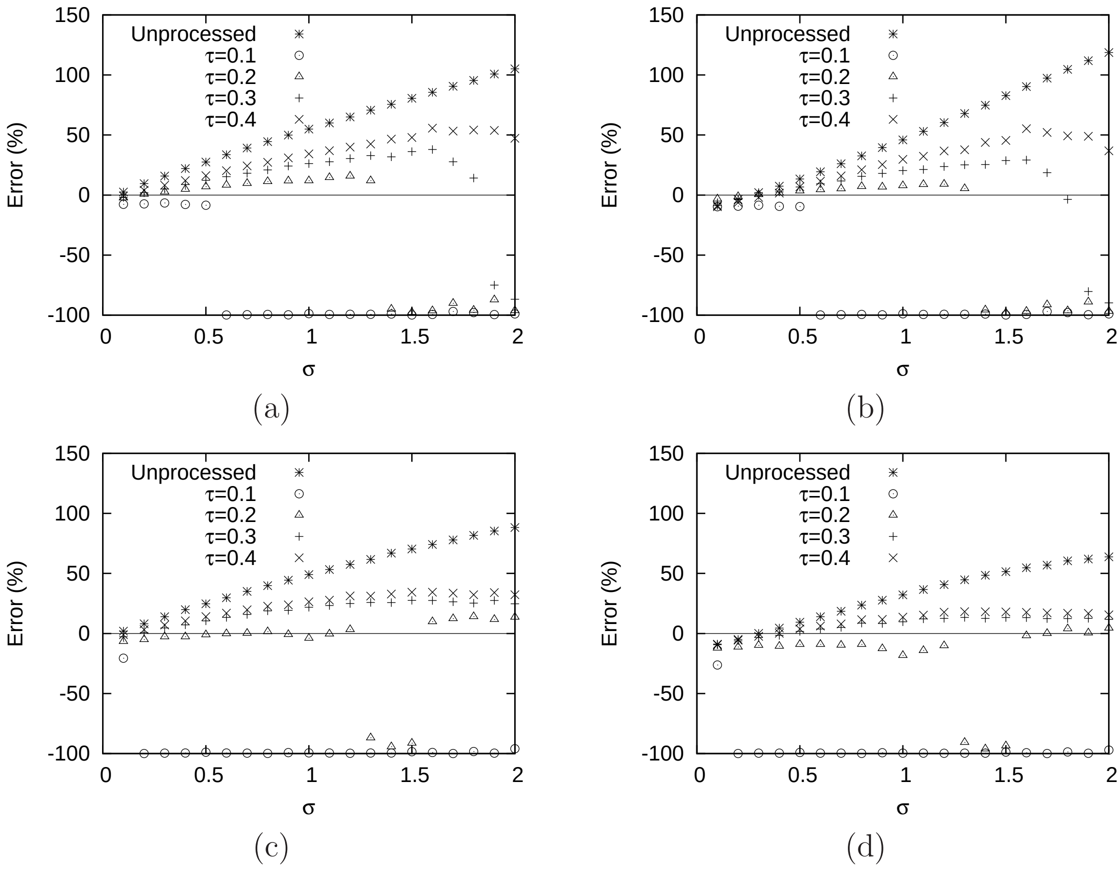

Figure 4: Percent error in the estimation of average diameter (a) and (c) volumetric, (b) and (d) numerical, as a function of σ for the unprocessed simulated disdrometer reading and for the proposed initial method for erroneous drop removal with different tolerances and for tests (a) and (b) 1, (c) and (d) 2.

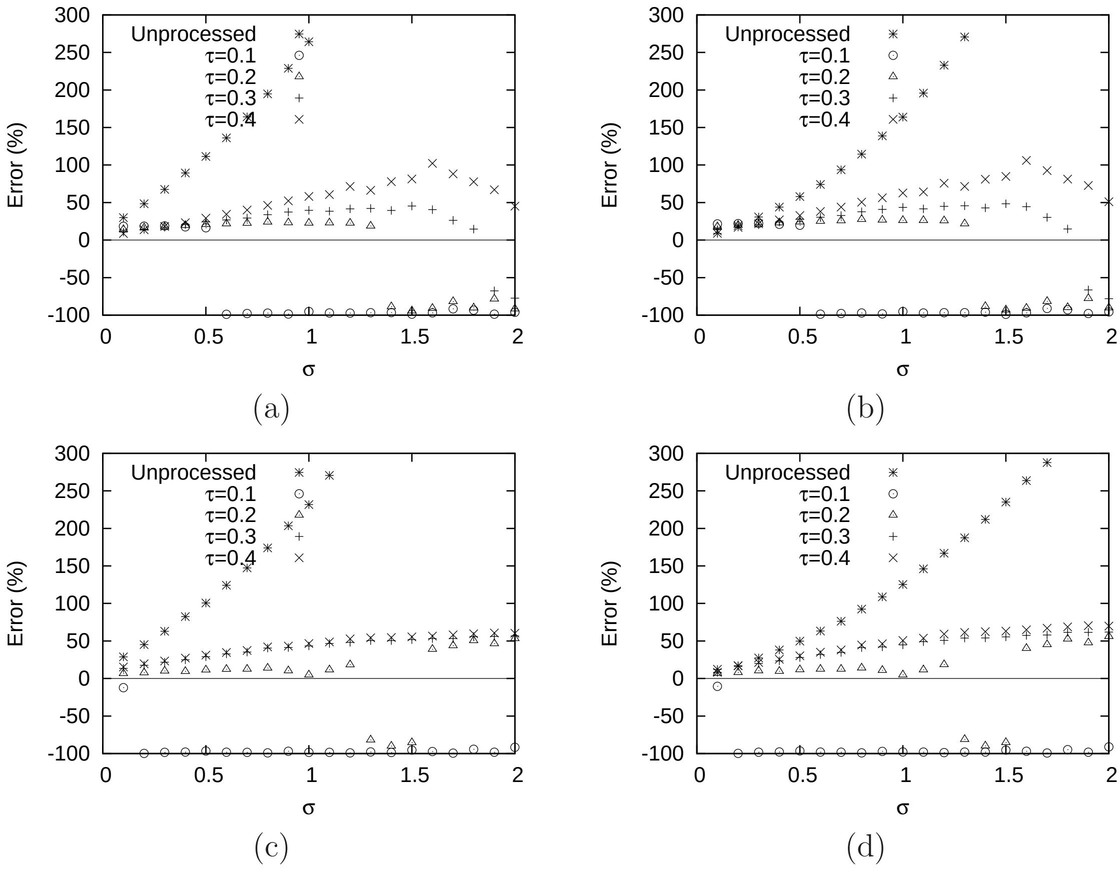

Figure 5: Percent error in the estimation of average time of passage (a) and (c) volumetric, (b) and (d) numerical, as a function of σ for the unprocessed simulated disdrometer reading and for the proposed initial method for erroneous drop removal with different tolerances and for tests (a) and (b) 1, (c) and (d) 2.

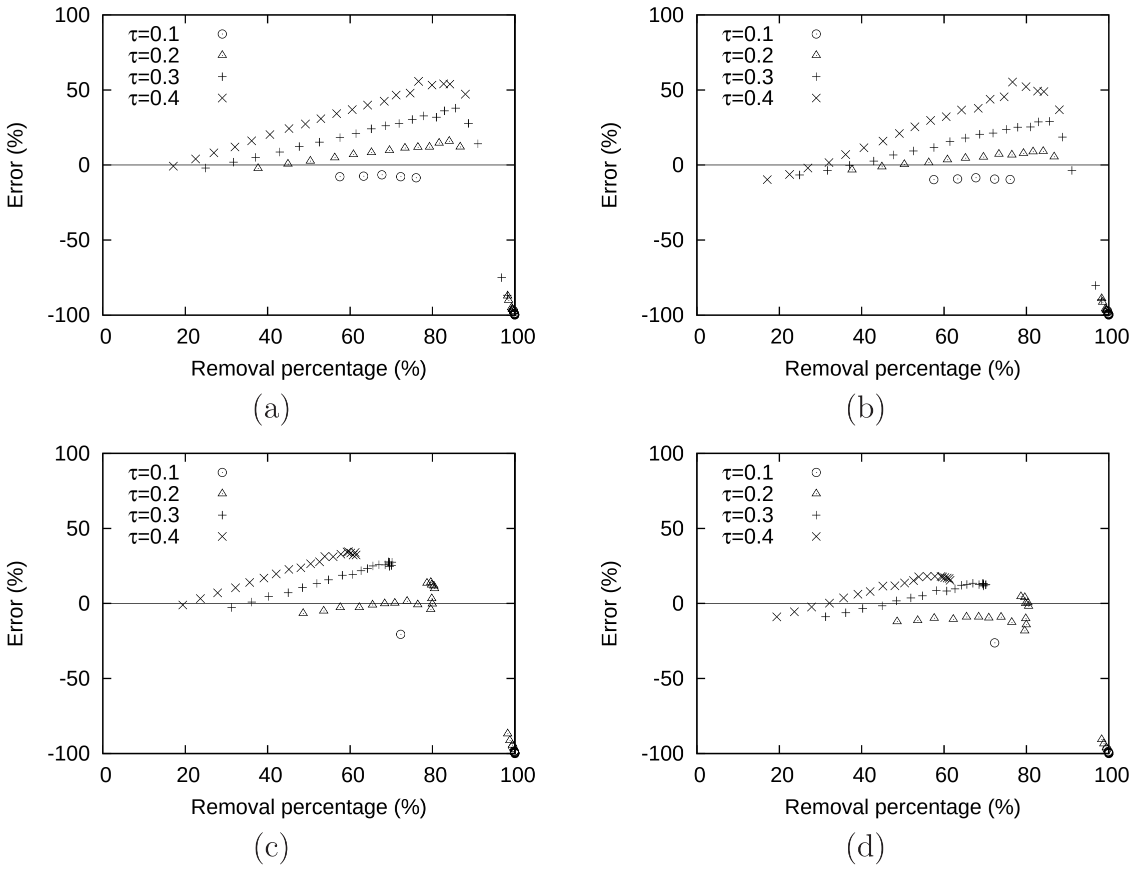

Figure 6: Percent error in the estimation of average diameter (a) and (c) volumetric, (b) and (d) numerical, as a function of the percentage of rejected drops for the unprocessed simulated disdrometer reading and for the proposed initial method for erroneous drop removal with different tolerances and for tests (a) and (b) 1, (c) and (d) 2.

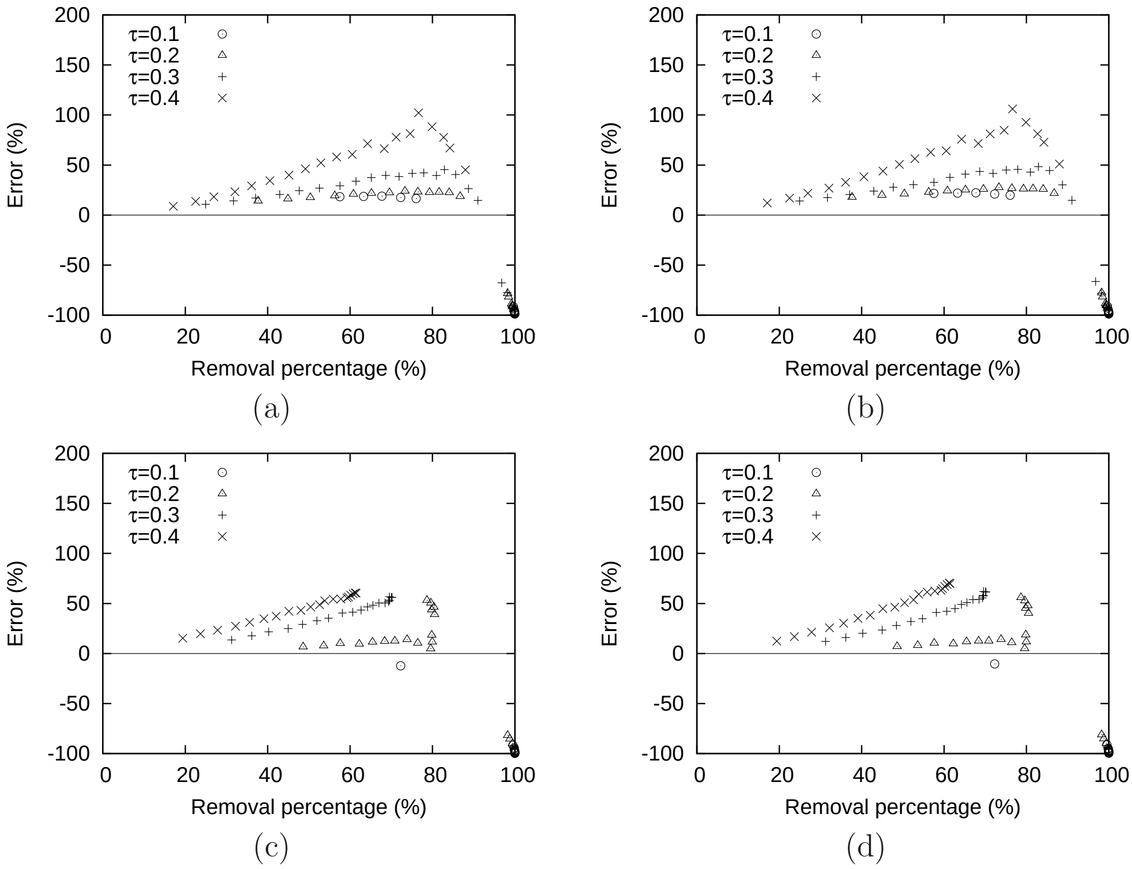

Figure 7: Percent error in the estimation of average time of passage (a) and (c) volumetric, (b) and (d) numerical, as a function of the percentage of rejected drops for the unprocessed simulated disdrometer reading and for the proposed initial method for erroneous drop removal with different tolerances and for tests (a) and (b) 1, (c) and (d) 2.

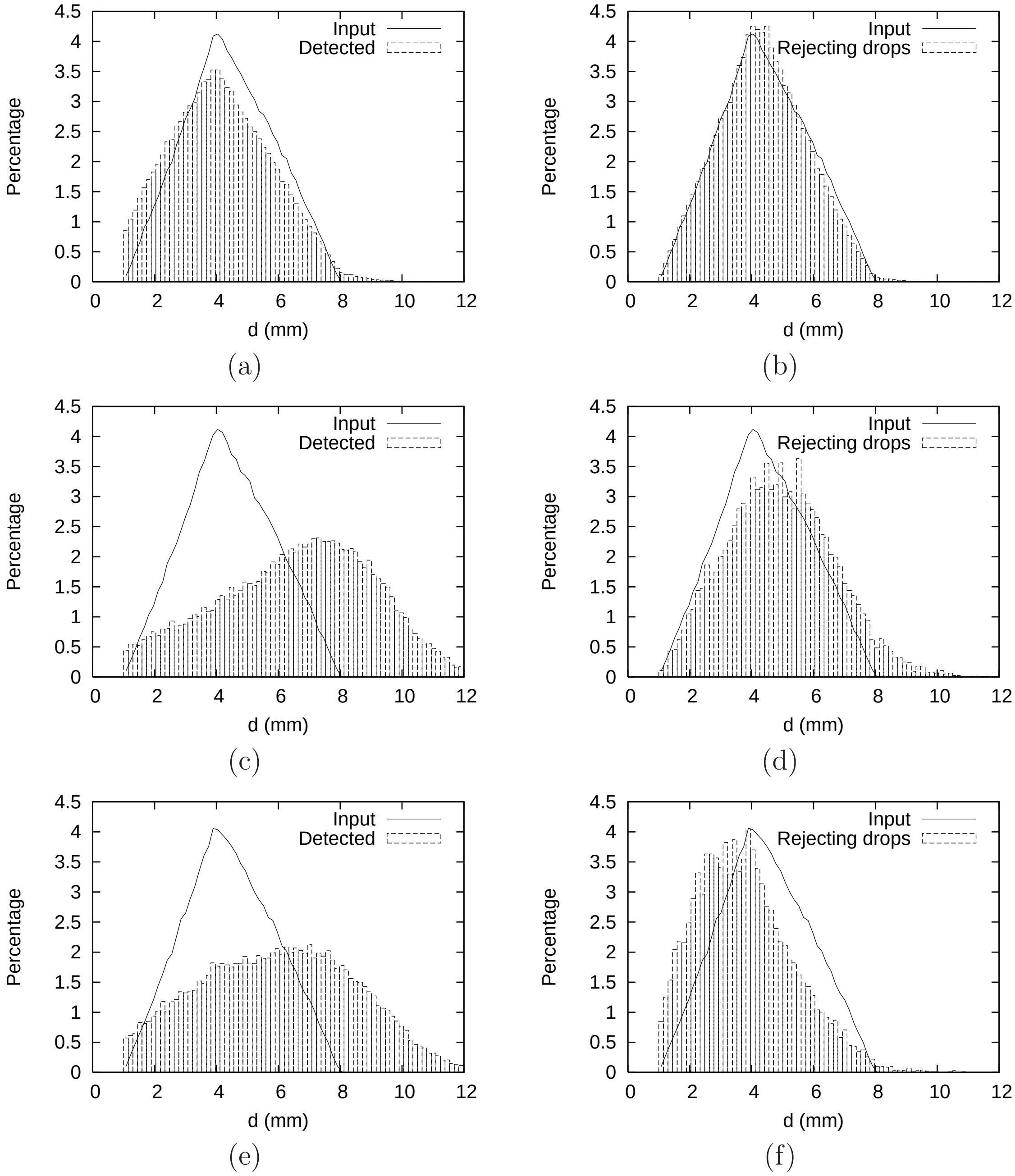

Figure 8: Histogram of drop diameter as detected by the disdrometer (a), (c) and (e), and as corrected using the improved method for drop rejection (b), (d) and (f). The relative drop density, σ, was 0.1 in (a) and (b), and 1 in (c), (d), (e) and (f). Test 1 (uniform drop velocity) was run in (a), (b), (c) and (d), while Test 2 (variable, random drop velocity) was run in (e) and (f). In all cases experimental histograms are compared with the real, triangular frequency distribution used in the numerical tests.

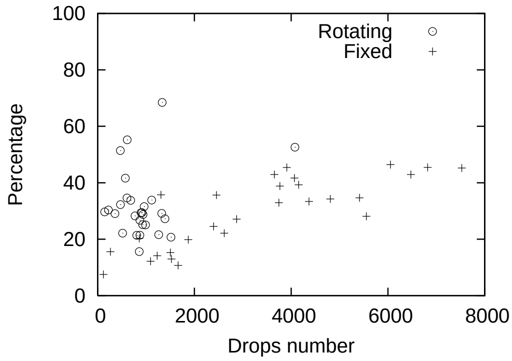

Figure 9: Percentage of drop removal with the improved method as a function of total number of detected drops for rotating and fixed sprinkler head.

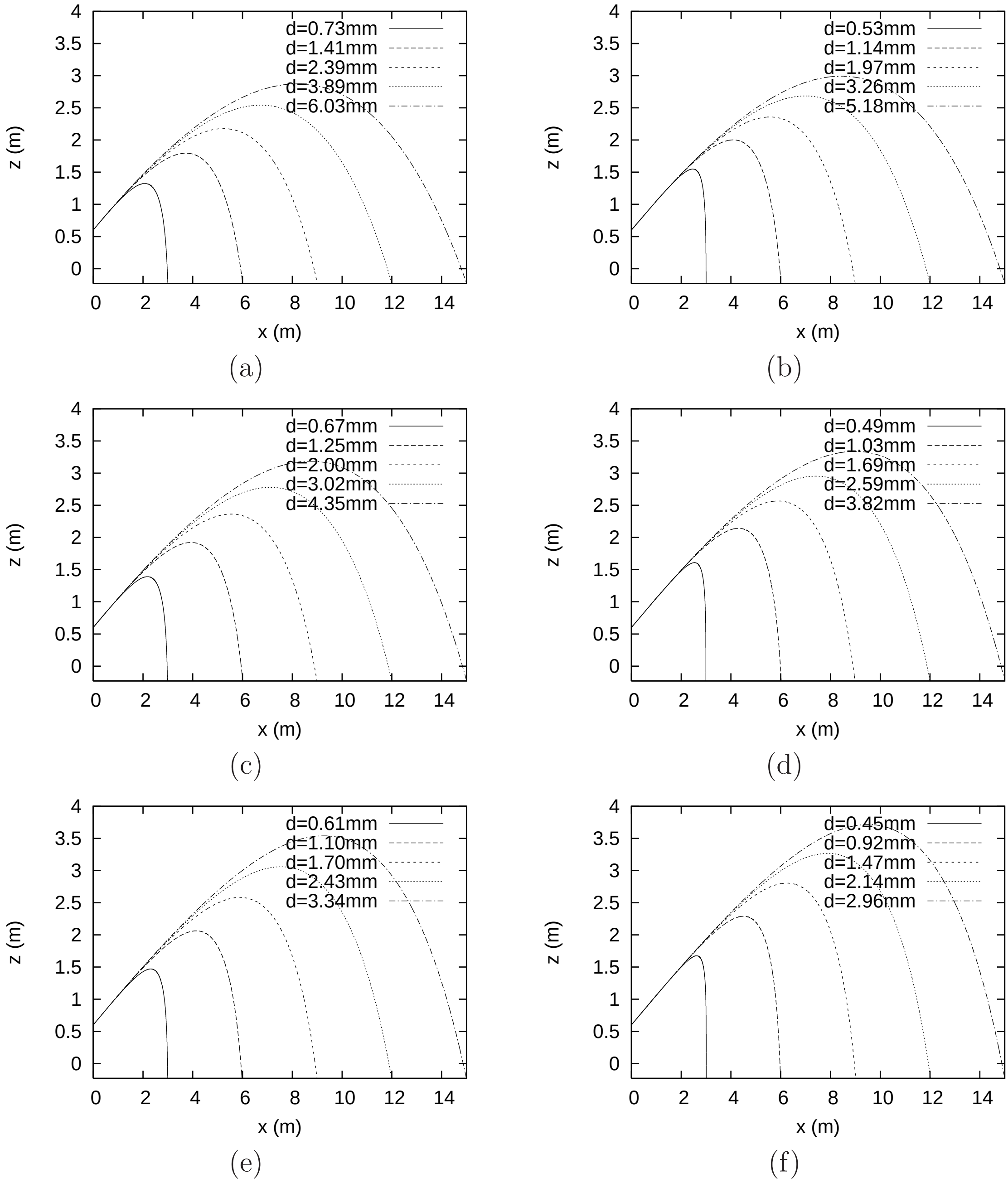

Figure 10: Simulated drop trajectories for pressures of (a) and (b) 200, (c) and (d) 300, (e) and (f) 500 kPa. In (b), (d) and (f) aerodynamic resistance was assumed zero for the first 1 m of the jet.

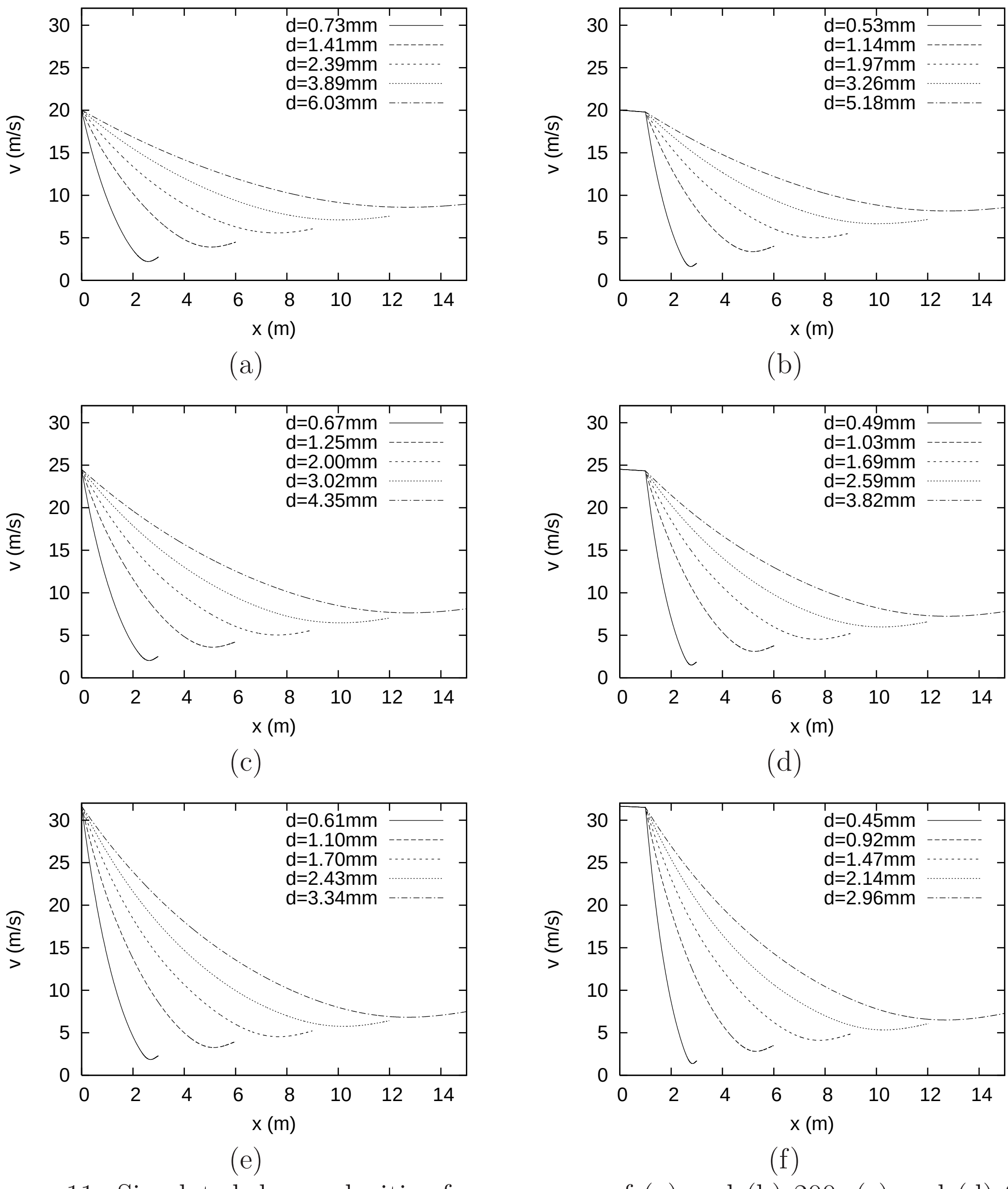

Figure 11: Simulated drop velocities for pressures of (a) and (b) 200, (c) and (d) 300, (e) and (f) 500 kPa. In (b), (d) and (f) aerodynamic resistance was assumed zero for the first 1 m of the jet.

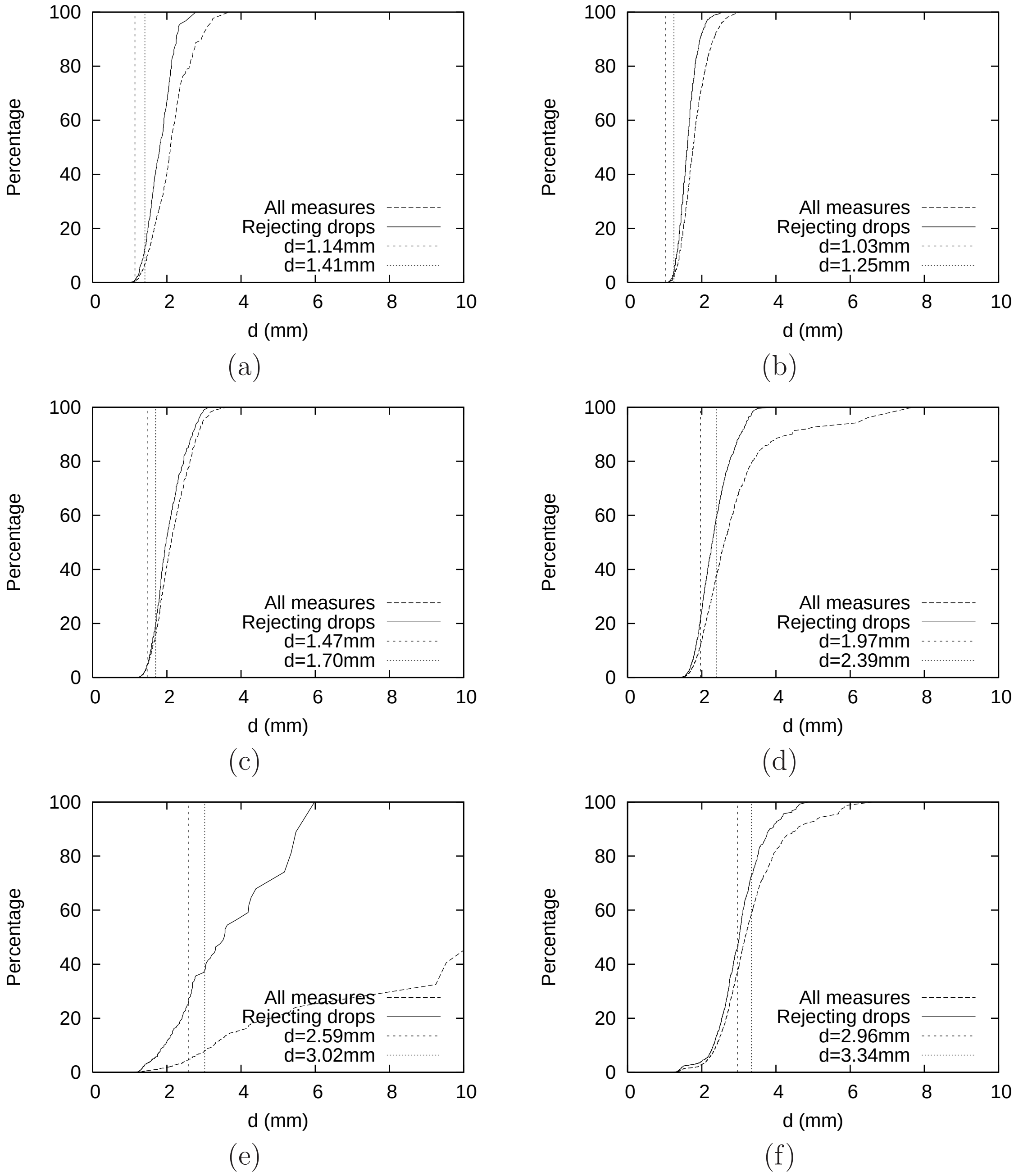

Figure 12: Percentage of emitted water volume as a function of drop diameter as measured with the disdrometer and as treated with the improved method for erroneous drop removal. These data are compared with the simulated drop diameters resulting in trajectories reaching the ground at the location of the disdrometer. These diameters are presented for a full drop trajectory (right) and for a 1 m compact jet before breaking out into drops (left). Results are presented for an operating pressure, for a distance to the sprinkler and for nozzle diameters of (a) 200 kPa, 6 m, 4.8 mm, (b) 300 kPa, 6 m, 6.0 mm, (c) 500 kPa, 9 m, 3.2 mm, (d) 200 kPa, 9 m, 4.8 mm, (b) 300 kPa, 12 m, 6.0 mm, (c) 500 kPa, 15 m, 3.2 mm. Sprinkler head rotated in (a), (c) and (e), and was fixed in (b), (d) and (f).

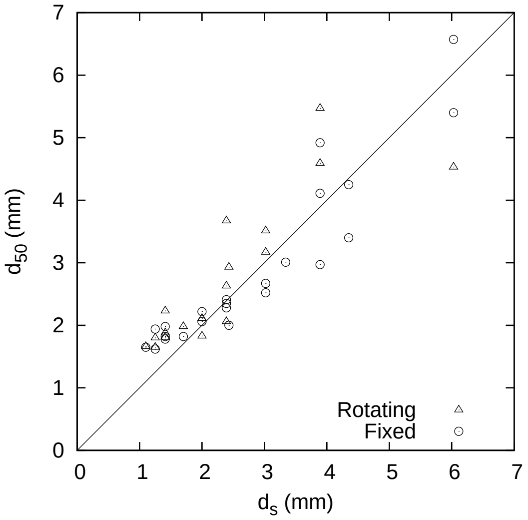

(a)

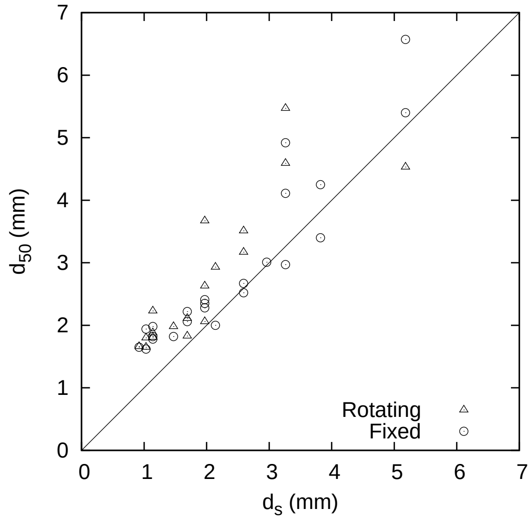

(b)

Figure 13: Simulated drop diameters ((a) without jet, (b) with a 1 m jet) vs. average corrected drop diameters (d_{50}) at different distances from the sprinkler. Results are presented for the whole experimental set, noting the experiments performed with fixed and rotating sprinkler head. The lines included in both plots have a 1:1 slope.

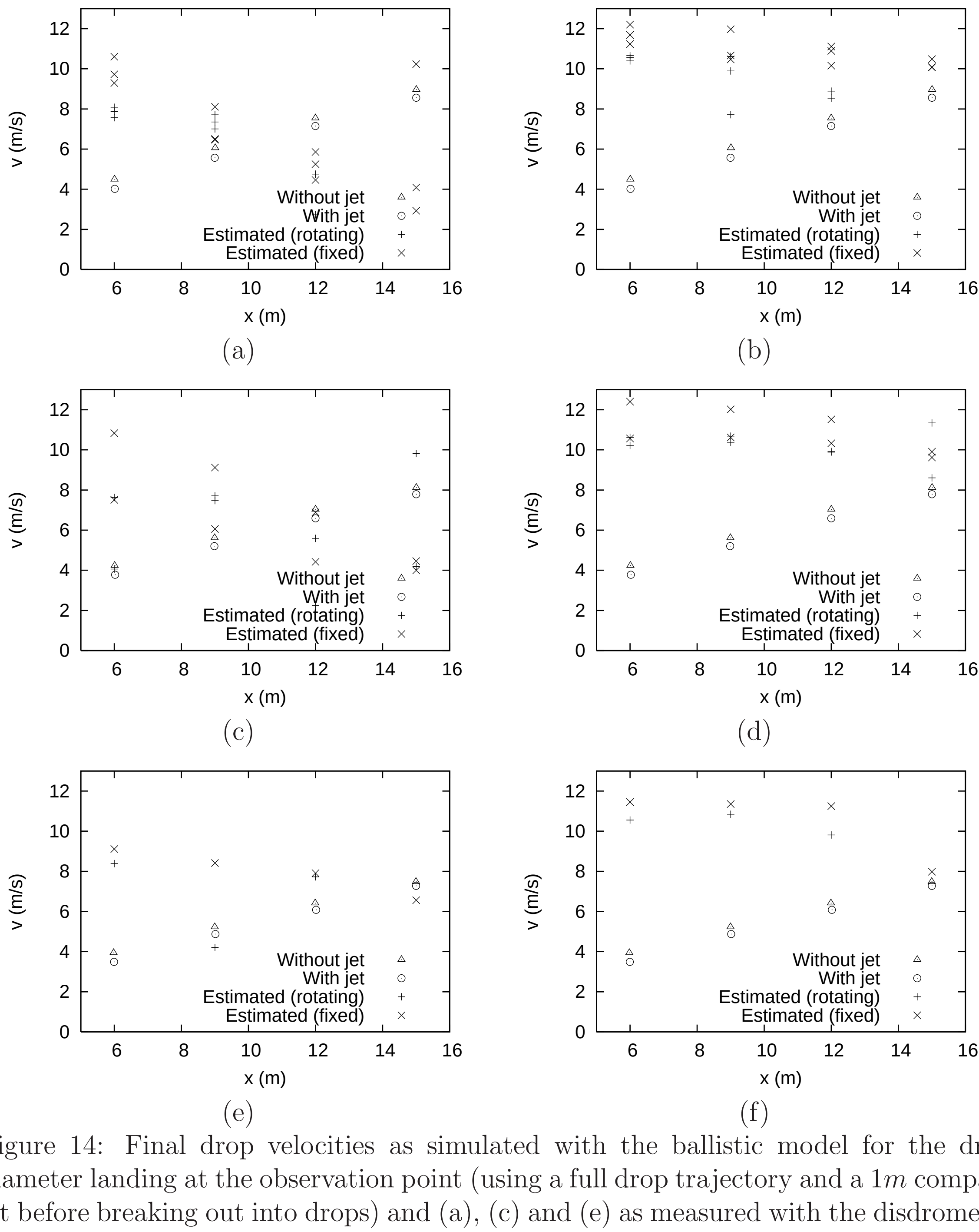

Figure 14: Final drop velocities as simulated with the ballistic model for the drop diameter landing at the observation point (using a full drop trajectory and a $1m$ compact jet before breaking out into drops) and (a), (c) and (e) as measured with the disdrometer (for the nozzles used in the experiments with a rotating and a fixed sprinkler head), (b), (d) and (f) using the improved method for erroneous drop removal. Results are displayed for the different distances to the sprinkler and for pressures of (a) and (b) 200, (c) and (d) 300, and (e) and (f) 500 kPa.